Surface air temperature fluctuations and lapse rates on Olivares Gamma Glacier, Rio Olivares basin, central Chile, from a novel meteorological sensor network

EDWARD HANNA

Department of Geography, University of Lincoln, UK

SEBASTIAN H. MERNILD

Nansen Environmental and Remote Sensing Center, Bergen, NORWAY; Antarctic and Sub-Antarctic Program, Universidad de Magallanes, Punta Arenas, CHILE; and Faculty of Engineering and Science, Western Norway University of Applied Sciences, Sogndal, NORWAY

JACOB C. YDE

Faculty of Engineering and Science, Western Norway University of Applied Sciences, Sogndal, NORWAY

SIMON de VILLIERS

Faculty of Engineering and Science, Western Norway University of Applied Sciences, Sogndal, NORWAY

Submitted to Advances in Meteorology, 3 March 2017.

Resubmitted, 16 May 2017

Corresponding author:

Professor Sebastian H. Mernild

Nansen Environmental and Remote Sensing Center, Bergen, Norway

Email: sebastian.mernild@nersc.no

Abstract

Empirically based studies of glacier meteorology, especially for the Southern Hemisphere, are relatively sparse in the literature. Here, we use an innovative network of highly-portable, low-cost thermometers to report on *high*-frequency (1-min time resolution) surface air temperature fluctuations and lapse rates (LR) in a ~800-m elevational range (from 3,675 to 4,492 m a.s.l.) across the glacier Olivares Gamma in the central Andes, Chile. Temperatures were measured during an intense field campaign in late Southern summer, 19–27 March 2015, under varying weather conditions. We found a complex dependence of high-frequency LR on time of day, topography and wider meteorological conditions, with hourly temperature variations during this week that were probably mainly associated with short- and long-wave radiation changes and not with wind speed/direction changes. Using various pairs of sites within our station network, we also analyze spatial variations in LR. Uniquely in this study, we compare temperatures measured at heights of 1-m and 2-m above the glacier surface for the network of five sites, and found that temperatures at these two heights occasionally differed by more than ±4°C during the early afternoons, although the mean temperature difference is much smaller (~0.3°C). An implication of our results is that daily, hourly, or even monthly-averaged LR may be insufficient for feeding into accurate melt models of glacier change, with the adoption of sub-hourly (ideally 1–10-min) resolution LR likely to prove fruitful in developing new innovative high-time-resolution melt modelling. Our results are useful potentially as input LR for local glacier melt models, and for improving the understanding of lapse-rate fluctuations and glacier response to climate change.

Keywords: Air temperature, Chile, glacier, lapse rate, melt, model, Olivares Glacier Gamma

1. Introduction

In recent decades, land-terminating glaciers and ice caps have thinned and receded in many regions of the world including Chile (e.g., Oerlemans et al. 2007; Rabatel et al. 2011, Cogley 2012; Leclercq and Oerlemans 2012; Malmros et al. 2016, Mernild et al. 2014). This is a visible response to climate variability and climate change, or more specifically changes in precipitation/snow accumulation and atmospheric warming. Glaciers in central Chile in the central dry Andes have shrunk and retreated rapidly during the last few decades due to a warming climate (Casassa 1995; Carrasco et al. 2005; Mernild et al. 2016), with serious impacts on water resources including drinking water and water for irrigation purposes, hydro-electric power, and future global and regional sea-level rise (Grinsted 2013). In central Chile the most notable feature of the changing climate from 1979 to 2006 was a strong contrast between the coastal region (surface cooling: -0.2°C decade^{-1}) and the Andes region (surface warming: 0.25°C decade^{-1}) (Falvey and Garreaud 2009; Mernild et al. 2016).

From a hydrological perspective glaciers are a reservoir of freshwater stored as ice, affecting water balance conditions (e.g., Malmros et al. 2016). In the central part of Chile (taken as the region between 30 and 38°S), hydrological and climatological research studies highlight a lack of information on glaciological mass-balance observations and processes (Favier et al. 2009, Masiokas et al. 2009, Rabatel et al. 2011; Mernild et al. 2015); yet such knowledge is crucial for understanding the role of glaciers in current climate and hydrological perspectives. In a generally warming climate, the annual glacier runoff will ultimately decline as reduced glacier area outweighs the effect of increased glacier melting (AMAP 2011). According to the World Glacier Monitoring Service (WGMS) (the organization maintaining and collecting information about glacier mass-balance observations globally), few glaciers in South America have meteorological and mass-balance observations for recent decades (WGMS 2012; Rabatel et al. 2013), and this implies a fundamental lack of

84 understanding of climatological and glaciological conditions in complex high mountain
85 terrain.

86 High-frequency observed surface air temperature lapse rates (LR) on glaciers and in
87 complex terrain are seldom reported. Lundquist and Cayan (2007) analyzed surface
88 temperature patterns in complex terrain in Sierra Nevada, indicating that a simple lapse rate
89 often gives a poor description of a high-frequency spatial temperature structure. Blandford et
90 al. (2008) evaluated daily and seasonal variations of surface air temperature LR in south-
91 central Idaho emphasizing high variability on both daily and seasonal timescales. According
92 to Minder et al. (2010), high-resolution gridding of climate data often relies on assumptions
93 such as a constant surface temperature lapse rate of 6.5°C km^{-1}, ignoring high-frequency
94 fluctuations in LR. This may have consequences for numerical weather prediction models
95 when forecasting surface air temperatures and LR in complex terrains mainly during the
96 winter season (Pagès and Miró 2010). It may also have implications for understanding the
97 impacts from inversion and Foehn effects in these terrains. Therefore, many snow and glacier
98 surface melt models use an assumed linear LR, for example on mean monthly or annual
99 timescales, to distribute near-surface air temperature observations from automatic weather
100 stations to locations at different elevations where meteorological observations are not
101 available (e.g., Liston and Elder 2006).

102 The present study arises from a four year-long Fondecyt project using a
103 multidisciplinary approach for the Rio Olivares basin, central Chile, to significantly improve
104 our overall understanding of meteorological, glaciological, and hydrological conditions. One
105 of the aims of the project is to observe and analyze high-frequency near-surface air
106 temperature fluctuations and conditions (not free-air lapse rates), including LR on Olivares
107 Gamma Glacier [near-surface lapse rates are more variable than free-air lapse rates (Harlow
108 et al. 2004)]. This feeds into further aims to develop and set up meteorological, glacier

surface mass-balance (SMB), and freshwater runoff models to determine the impact of high-frequent fluctuations in surface air temperature LR and of climate change upon glacier SMB and spatiotemporal freshwater runoff conditions under present day climate change conditions. The present work on glacier micrometeorology, together with improved models of meteorological and glacier SMB, will allow us to better understand the impacts from present climate conditions on glaciological and hydrological conditions in Central Chile, and the complex interactions between these elements.

2. Study site

The Olivares Gamma Glacier (11.5 km^2 in 2012; 33°07'S, 70°10'W) (Figure 1) is located in the Rio Olivares basin (548 km^2), in Central Chile, *c.* 50 km northeast of Santiago de Chile, the capital city of Chile (7–8 mill. inhabitants). The Rio Olivares Basin contains *c.* a quarter of all the glacierised area feeding into the Rio Maipo basin, which provides water to Santiago de Chile and a substantial part of the Central Valley. The Olivares Gamma Glacier (hereafter referred to as Gamma) is a temperate glacier with a maximum thickness of 183 m water equivalent (w.e.) and an estimated water volume of 0.62 km^3 w.e. (DGA 2011). Gamma extends from 3,650 to 4,800 m a.s.l., and is facing south (Figure 1) (Malmros et al. 2016). No debris-covered glacier ice is present at Gamma. The glacier surface is characterised by fields of penitentes (ice pinnacles formed by evaporation-melt processes on high-altitude, low-latitude glaciers), generally less than 0.5 m in height.

3. Methods

We used ten Tinytag sensors, model Tinytag Plus 2 = TGP-4017, deployed in small plastic radiation shields (model no. ACS-5050) mounted on individual stakes, with sensors placed at 1-m and 2-m height above the glacier surface at each site. The relatively low cost of

a Tinytag temperature sensor, in comparison to an automatic weather station, meant that it was practicable to deploy ten Tinytags at five sites across the glacier (Figure 1). The equipment setup for two stations is shown in Figure 2. Station locations spanned an elevational range of ~800 m, which covered most of the glacier (Figure 1); elevation, slope, aspect, sensor ID numbers and observation times are given in Table 1. These temperature loggers can store up to 32,000 readings, and are suitable for deployment in the field for ~6–12 months; they have successfully been deployed in the sub-Arctic in previous studies (e.g., Yang et al. 2012).

Temperatures were logged at 1-min intervals, loggers were synchronised before deployment in the field, and all times reported in this paper are GMT/UTC (during the Austral, summer Chile is GMT -4 hours). Before being used in the field, the Tinytags were calibrated and validated against a full United Kingdom Accreditation Service (UKAS) Calibrated Max Min Thermometer, which had been calibrated to national standards using an independent calibration laboratory and was supplied with a traceable three-point calibration certificate taken at 0°C, 10°C, 25°C full UKAS standards and a cited accuracy of 0.1°C. Over a 15°C temperature range, the Tinytags agreed on average to within +0.1–0.4°C of the reference thermometer, with a mean difference of +0.2°C. These combined accuracies are within the Tinytag manufacturer's quoted accuracy of ±0.5°C for a 0–20ºC temperature range.

We also used a supplementary LogTag TRIX-8 Temperature Recorder in each screen, which automatically logged air temperature at 2-min intervals, to support the main temperature dataset. The LogTags store a slightly lower number of readings (8,000; hence the lower time resolution used here) but are considered by the manufacturer to be accurate to ±0.5°C for -20°C to +40°C, i.e. similar to the quoted accuracy of the Tinytags.

158 The Tinytag and LogTag temperature data were supplemented by an automatic
159 weather station (AWS) (Station DGA) located at 3,631-m elevation in the proglacial
160 landscape in front of the glacier (Figure 1). This provided hourly readings not just of air
161 temperature but also relative humidity, barometric pressure, wind speed and direction, and
162 incoming/outgoing short- and long-wave radiation, which helped place our distributed air
163 temperature records in a wider meteorological context.
164 We use standard descriptive statistics and correlation analysis to summarise
165 observational results and compare key datasets. Lapse rates are expressed as positive when
166 temperatures decrease with height, and negative when temperatures increase with height.
167
168 **4. Results and discussion**
169 *4.1 General weather conditions*
170 Figure 3a shows the meteorological data recorded at DGA during the fieldwork
171 campaign. Daily temperatures ranged from ~3-4°C (during night) to ~12-13°C (during day)
172 during the first few days then declined to -3-0°C to ~4-10°C during the latter part of the
173 campaign. These temperature changes were mirrored by opposite changes in relative
174 humidity (RH) to near-saturated air masses (~70–100% RH) during the latter half of the
175 period, with RH having risen from a relatively dry air-mass of 20–50% saturation during the
176 first few days (Figure 3a). Surface air pressure dropped from ~666 hPa in the first two days to
177 ~658–662 hPa in the days thereafter, reaching a minimum of <658 hPa on 25 March (Figure
178 3b). Winds were generally fairly light (~1–6 m s^{-1} for 10-min averages) and the wind was
179 predominantly north-westerly during the first half of the period, turning more variable and
180 mainly to a southerly point afterwards (Figure 3c). Incoming solar radiation peaked at
181 between 700–900 W m^{-2} during the first half of the period, with relatively low peaks around
182 500–600 W m^{-2} on 23 and 24 March. Longwave radiation, both incoming and outgoing,

183 varied most during the first few days, reflecting clearer skies, stronger surface heating during
184 daylight hours and greater heat loss in night time (Figure 3d).
185
186 *4.2 Glacier near-surface hourly temperatures and lapse rates and comparison with DGA*
187 *meteorological data*
188 A comparison of DGA hourly surface air temperature with 2-m temperatures at the
189 five Tinytag sites is shown in Figure 4. Figure 4a confirms a steady temperature decrease at
190 all sites throughout the week-long period. DGA daytime peaks tended to occur 1–2 hours
191 after temperature peaks at the Tinytag sites (Figure 4b). Mean hourly temperatures data for
192 the DGA and Tinytag sites for 22–26 March 2015 are shown in Table 2 and Figure 4b. DGA
193 temperature ranged from 0.2°C at 10:00 to 7.0°C at 18:00; the nearest Tinytag 2-m Station S2
194 ranged from -0.1°C at 11:00 to 8.5°C at 17:00. At 11:00, on average, 2-m temperatures at five
195 out of six sites were below freezing (except for DGA = 0.5°C). Overall, mean hourly
196 temperatures (mean of all 24 hours) for these five days were similar at 2.7°C and 2.5°C for
197 DGA and S2, although temperature variations were greater at S2, with a standard deviation of
198 2.5°C for all hourly data compared with 1.9°C at DGA. Mean hourly temperatures at the
199 highest site S4 (4,492 m) were only slightly above freezing (0.2–1.0°C) at three hours,
200 16:00–18:00, compared with 23 hours for the lowest Tinytag site S2 and all hours at DGA
201 (Figure 4b). This suggests that there was not much melting on the upper reaches of the glacier
202 around Station 1 (S9/S4) during the study period. However, mean daily 2-m temperatures
203 were above freezing (1.1°C at S6 and 2.5°C at S2) for the lowest two Tinytag stations. The
204 highest mean hourly temperatures (at 17:00) of 8.5°C and 8.1°C at the same two sites were
205 substantially above the mean hourly temperature of 5.4°C at the lower DGA site (which
206 occupies much darker moraine and bedrock well below the glacier terminus). This could be

207 due to strong reflected solar radiation enhancing surface air temperature readings (even
208 though they were obtained from properly screened thermometers) at the Tinytag sites.
209 Mean hourly (22–26 March 2015) lapse rate data for various pairs of 2-m sensors are
210 given in Table 3. In that table, the second from left column LR (S4-S2) shows the full-range
211 lapse rate between the 2-m Tintags at Stations 1 and 5, which are separated by 817 m in
212 elevation (Figure 1; Table 1). This shows the strongest lapse rates, commonly <-10.0 °C km^{-1}
213 , during the early afternoon hours, with hourly lapse rates generally between about -7 and -
214 8°C at other times. Therefore, these lapse rates were mainly slightly smaller than the dry
215 adiabatic lapse rate (DALR) of -9.8°C km^{-1}, and it was only at 15:00 that the DALR was on
216 average exceeded (greater negative values). These super-adiabatic lapse rates could be due to
217 preferential warming of lower slopes under conditions there of greater ice-melt and lower
218 albedo, hence more absorption of incoming solar radiation. Sub-profiles between pairs of
219 stations reveal occasional much stronger mean hourly lapse rates: e.g., -16.6 °C km^{-1} for S5-
220 S6 (Station 3 – Station 4) at 17:00 and -13.0°C km^{-1} for S6-S2 (Station 4 – Station 5) at 15:00
221 for the six days. Large reductions (smaller negative values) in lapse rates at some sites were
222 evident for the mid-afternoon hours. These include most notably reductions in the S3-S2
223 (Station 2–Station 5) lapse rate from -10.1°C km^{-1} at 15:00 to -0.3°C km^{-1} at 18:00, the S3-S6
224 (Station 2–Station 4) lapse rate from -11.5°C km^{-1} at 17:00 to -1.2°C km^{-1} at 18:00, and the
225 S6-S2 (Station 4–Station 5) lapse rate from -13.0°C km^{-1} at 15:00 to 1.5°C km^{-1} at 18:00
226 (Table 3). The latter case is the only reversed (negative) lapse rate value in the whole of
227 Table 3, where the normal lapse rate profile (temperature decrease with height) temporarily
228 changes sign at 18:00 on average over the six days (there is another, already mentioned near-
229 neutral lapse rate of -0.3°C km^{-1} for S3-S2 at the same time).
230 These early afternoon large drops/reversals in lapse rates are mainly related to the
231 diurnal temperature peaking one hour later at S3 (Station 2) compared with the lower S6

(Station 4) and S2 (Station 5) – and indeed the other two S4 and S5 2-m Logtag – sites; the only other site with peak temperature at 18:00 (in common with S3/Station 2) is DGA. Why do these two sites' daily temperatures peak later than the others? There is nothing especially unusual about the slope and aspect of Station 2 compared with the other four stations (Table 1). As is clear from Figure 1, both Stations 2 and 3 are located fairly near the mid-point/centre line of the glacier, so anomalous shading from surrounding topography at Station 2 is not an issue [especially at this time of the year/local time of day, early afternoon, when the Sun was high in the (northern) sky]. Figure 2a and 2b shows photos of both sites: the glacier surface at Station 3 appears significantly rougher and possibly consequently darker than Station 2, so it could be that a local effect of the glacio-morphology influences the surface energy balance, and this effect may delay the timing of the peak daily temperature at Station 2. We postulate that this is because the generally smoother, brighter ice surface at Station 2 takes longer to respond to increasing solar radiation during the first half of the day. The 2-m night-time temperatures at S3 (Station 2) and S5 (Station 3) are very similar but mid-afternoon temperatures are much higher at S3 (by over 2°C at 18:00, Table 2), even though they peak slightly later. These differences emphasise the importance of local glacier surface microstructure on the 1 cm to 10 m spatial scale, compared with broader-scale topography, in affecting surface air temperature daily peaks and the timings of these. Heterogeneous surface microstructure has an impact on both the spatial and temporal variability in lapse rates, as illustrated above. In agreement, Blandford et al. (2008), working in mountainous regions in south-central Idaho, showed that different synoptic weather types influenced surface lapse rates, where for example warmer air temperatures were associated with steeper lapse rates and vice versa.

Correlations between hourly temperature data and meteorological parameters recorded by the DGA AWS are given in Table 4. These show significant strong positive

correlations between Tinytag temperatures and DGA air temperature, incoming shortwave radiation and outgoing longwave radiation but little/insignificant correlation between Tinytag temperatures, for any of the sites, and wind speed and direction recorded at DGA. This suggests that glacier surface air temperatures during the week-long period in question were regulated mainly by key radiative components of the surface energy balance and very little by advective processes (wind). While the wind speed data recorded at DGA suggest that wind does not have an impact on lapse rate, we cannot exclude the possibility that there could be micro-scale advection occurring along the glacier – particularly in those short periods when lapse-rates become very high for a few minutes. Some kind of upslope convection is necessary to stabilize the atmosphere along-slope. Given that there are no high-frequency wind measurements along the slope of the glacier in this study, advection cannot be entirely discounted. Although our findings are only for a week-long period due to practical fieldwork constraints, Pepin et al. (1999) conducted a study in the uplands of northern England evaluating surface air temperature lapse rates, highlighting that steep lapse rates occurred with higher levels of solar radiation, but also that wind speed during the day had relatively little impact on lapse rates, in agreement with our results.

4.3 Comparison of temperatures at 1-m and 2-m heights above glacier surface

We also compare Tinytag temperatures recorded at 2-m and 1-m heights. Differences between these are generally small 0.1–0.4°C, but occasionally exceed 1°C based on mean hourly data (Table 5). Figure 5a shows occasional 2-1 m air temperature differences for individual days as great as ±4°C based on 1-min data. For the mean daily profile, greatest differences were between 13:00 and 20:00 UTC, and briefly exceed 1.5°C at S6-S7 (Station 4) based on 1-min data (Figure 5b). Figure 5a shows occasional 2-1 m air temperature differences for individual days as great as ±4°C based on 1-min data. Differences are

generally negative (higher temperatures at 2 m) but positive in mid-afternoon (local time) at S5-S10 and S3-S8 (Stations 2 and 3). The greatest negative differences are for S6-S7, S4-S9 and S2-S1 (Stations 4, 1, and 5) in mid-afternoon.

The generally greater temperatures at 2-m can be attributed to boundary-layer effects of a cold ice surface having a stronger influence on suppressing air temperatures nearer the surface during daytime, especially under conditions of strong solar radiation, and heat loss through infrared radiational cooling lowering the surface temperature more during night time. The latter effect appears to have prevailed under clear night skies during the first half of the period (19–23 March 2015), as thereafter the night-time temperature bias was mainly much closer to zero (Figure 5a). Local site characteristics, such as albedo and topographic roughness, and/or meteorological changes, for example local-scale micro-advection, may explain the opposite sign of 2-1 m temperature differences during mid-afternoon at Stations 2 and 3, since temperature differences at all five sites were systematically slightly positive at other times of the day.

The good agreement of the systematic positive temperature bias from 23:00 to 12:00 supports the good relative accuracy/calibration of the Tinytags (discussed above). The 1-min data also show rapid variation of 2-1 m vertical lapse rates for several hours in mid-afternoon, reflecting rapid changes in the boundary-layer profile and energy exchanges between the atmosphere and surface: this effect was most marked on 24 and 25 March – a time of more unsettled weather conditions, lower solar radiation and more variable wind (Figure 3).

4.4 Analysis of high-frequency (1-min) temperature and lapse-rate data

In this section we carry out a more detailed analysis of the 1-min data from the Tinytags, which are presented in Figures 6–8. Daily mean and mean daily (22–26 March 2015) temperatures for all ten Tinytag sensors (1-m and 2-m elevation at five sites) are

307 reported in Table 6, and daily mean and mean daily lapse rates between various pairs of
308 Tinytags are given in Table 7. Near surface air temperature lapse rates for the full elevation
309 profile (S4-S2 at 2-m and S9-S1 at 1-m height above the surface) were on average ~1.5–
310 2.0°C km^{-1} lower on 24 and 25 March than the other days. This was during the unsettled
311 weather period when relative humidity (as indicated by DGA) was much higher, indicating a
312 near-saturated air mass. Since saturated air cools at a lower rate as it rises than non-saturated
313 air (as latent heat is released to its surroundings), this may explain the smaller lapse rates
314 measured on 24/25 March. Although here we are looking at the near-surface lapse rate of the
315 glacier surface rather than the free-air lapse rate of a rising air parcel, these two lapse rates
316 can be related. The smallest daily mean lapse rates of -3.1°C km^{-1} and -3.3°C km^{-1} are seen
317 for S6-S2 and S7-S1 (both are Stations 4-5) on 24 March (Table 7). This more moderate
318 lapse rate on the lower reaches of the glacier may also be related to changes in the surface
319 energy balance under more cloudy, humid weather conditions. The lapse rates on the upper
320 reaches on the glacier (S4-S3 and S9-S8) are below -10°C km^{-1}, which are some of the
321 steepest lapse rates recorded. Figure 6a is a much higher-time resolution version of the
322 temperature data in Figure 4a (but does not include DGA data). Although the two graphs look
323 rather similar, Figure 6a shows striking short-term (minutes-timescale) temperature
324 fluctuations that are hidden in Figure 4a. For example, a ~4°C temperature drop at S2 is
325 clearly visible just before the daily temperature peak on 26 March in Figure 6a is almost
326 completely smoothed out in Figure 4a; a similar feature is seen in the S1 profile in Figure 6b.
327 These short-term temperature fluctuations contribute to brief blips in the lapse-rates
328 shown in Figure 7 of as high as ±30–50°C km^{-1} for several minutes, generally in the early
329 afternoons: these are most marked for the S6-S2 and S7-S1 (Stations 4 and 5) sub-profile on
330 the lower part of the glacier and are much more modest (~0– -20°C km^{-1}) for the full vertical
331 profile (S4-S2 and S9-S1, Stations 1 and 5). Figure 8 shows the mean daily lapse rate profiles

for various pairs of sites (e.g., between 2-m Tinytags in Figures 8a and 8c and 1-m Tinytags in Figures 8b and 8d). Figure 8e shows lapse rates for both the 2-m and 1-m Tinytags for the upper half of the glacier. Large fluctuations in the lapse rates in the early-mid afternoon (local time) dominate all the plots in Figure 8, in contrast to relatively stable lapse rates at other times of the day. The temporary lapse-rate reversal from negative values to positive values for the lower two sites, best shown here for the S6-S2 2-m profile (Figure 8a) has been remarked on above (Section 3.2) but is now shown in much more detail – especially regarding the extreme values reached – based on the 1-min Tinytag data. Here, for S6-S2 we see a spike going up to +5°C km^{-1} (Figure 8a), which, because it occurred between hours, is not apparent in the mean hourly lapse rate data in Table 3. The relatively large fluctuations in the afternoon lapse rates tend to be greater for the Tinytags at 2 m compared with those at 1 m (Figures 8a–8d), indicating an atmospheric influence with stronger decoupling from the surface at the higher height.

4.5 Comparison of Tinytag and Logtag temperature data

The main Tinytag temperature data were compared with a supplementary LogTag temperature sensor that was also included in each screen. Mean temperature differences of LogTag minus Tinytag temperatures for 22–26 March are shown in Table 8 and Figure S2, and the whole time series are in Figure S1 (Supplementary Information). For nine out of ten instrument sites, these differences are within ±0.3°C, with an overall mean difference of +0.2°C. This small temperature difference was analysed by time of day, and was found to be greatest at +0.5°C for 12:00–15:00 GMT, i.e. mid-late morning local time, and least at 0.0°C at 18:00–21:00 GMT. These differences are mainly within instrument error but the LogTag mid-late morning warm bias was accentuated at a couple of sites, i.e. for S7 was +1.0°C at 12:00–15:00, +1.3°C at 15:00–18:00, and +0.9°C at 18:00–21:00. The S9 LogTag warm bias

was +0.7°C at 12:00–15:00 and +0.8°C at 15:00-18:00. These slightly larger temperature differences at a couple of sites are either on the threshold of or slightly exceed instrument error, and show an occasional tendency for the Logtags to give slightly higher temperatures than the Tinytags around midday. However, this small difference is apparently spatially random and not systematic across all sites. Figures S1 and S2 respectively show comparisons of the Tinytag and LogTag temperature time series and mean daily temperature cycles, showing generally very good agreement at all sites. This very good agreement between the two independent sets of instruments, in addition to the absolute calibration procedure for the Tinytags described above, gives us high confidence in our results regarding near-surface glacier temperature lapse-rate values and changes.

5. Summary and conclusions

Our results show that near-surface lapse rates on Glacier Gamma were generally greater under clear/sunny weather conditions – especially in early afternoon – and decreased during a period of more unsettled, cloudy weather later on in the fieldwork, displaying similar trends to those reported for a mountainous region in south-central Idaho (Blandford et al. 2008). Temperatures at 1-m and 2-m heights above the surface are generally similar, within 0.5°C, but occasionally vary by as much as ±4°C, depending on changes in the surface energy budget and in the ambient meteorological conditions. This makes it critical to document at what height temperatures are being recorded in any study of high-resolution glacier meteorology (most such studies do not measure air temperature at multiple heights). Our relatively low-cost Tinytag network was able to resolve these vertical temperature changes, as well as spatial/elevational changes in temperatures and lapse rates, at the 1-min timescale, in a dataset that is rarely available for whole glaciers, let alone a glacier in South America or Chile. A natural extension of this study could use suitably mounted and shielded

Tinytags to acquire temperature data over the course of 6–12 months, albeit at a slightly decreased sampling time resolution (e.g., 15–30 min), due to the large Tinytag logger capacity (32,000 number of readings). This will provide a better understanding of the monthly, seasonal and higher-time-resolution variabilities in lapse rates, since most models use linear LR assumptions on mean monthly to annual scales. Another consequence of our findings is that lapse rates – especially in daytime – can be highly spatially and temporally variable (at the 1-min to 1-hour timescale) across a small glacier, and therefore computer models of glacier melt can benefit significantly through having this kind of high-resolution information on surface air temperature lapse rates.

Moreover, we suggest that the assumption of linear lapse rates in glacier melt models appears not to be valid, at least on the sub-hourly timescale, and meteorological monitoring of a glacier should ideally include multiple temperature loggers along the vertical profile to capture these spatial/temporal inhomogeneities. Therefore, the kind of data here – especially if extended to longer time periods and/or more glaciers – can be used in a sensitivity study to help trial and develop glacier melt models as well as for improving understanding of glacier meteorology and glacier interaction with climate change.

Acknowledgments

The authors acknowledge financial project support from the Chilean government (Fondecyt Regular project number: #1140172). Also, we thank JSPS (Japan Society for Promote Science) for support, under project number: #S17096. E.H. would like to thank the University of Sheffield for the granting of a sabbatical, which enabled him to join the fieldwork team and pursue this research.

References

AMAP (2011). Snow, Water, Ice and Permafrost in the Arctic (SWIPA): Climate Change and the Cryosphere. Chapter 7: Mountain Glaciers and Ice Caps, 61 pp. Arctic Monitoring and Assessment Program (AMAP), Oslo, Norway, xii + 538 pp.

Blandford, T., K. Humes, B. Harshburger, B. Moore, V. Walden, and H. Ye (2008). Seasonal and synoptic variations in near-surface air temperature lapse rates in a mountainous basin. *Journal of Applied Meteorology and Climatoligy*, 47(1), 249–261, doi:10.1175/2007JAMC1565.1.

Bolstad, P. V., Swift, L., Collins, F., and Regniere, J. (1998). Measured and predicted air temperatures at basin to regional scales in the southern Appalachian mountains. *Agric. For. Meteorol.*, 91(3-4), 161–176.

Carrasco, J. F., Casassa, G. & Quintana, J. (2005). Changes of the 0°C isotherm and the Equilibrium line altitude in central Chile during the last quarter of the 20th century. *Hydrological Sciences/Journal des Sciences Hydrologiques* 50, 933–948.

Casassa, G. (1995). Glacier inventory in Chile: current status and recent glacier variations. *Ann. Glaciol.* 21. 317–322.

Cogley, J. G. (2012). The future of the world's glaciers. Pp. 197–222 in A. Henderson Sellers and K. McGuffie, editors. The Future of the World's Climate. Elsevier, Amsterdam. The Netherlands.

DGA (2011). Estimacion de volumenes de hielo en glaciers de Chile Central. Direction de Aguas. SIT 264 (1), pp. 155.

Falvey, M., and Garreaud, R. D. (2009). Regional cooling in a warming world: Recent temperature trends in the southeast Pacific and along the west coast of subtropical South America (1979-2006). *J. Geophys. Res.* 114, D04102, doi:10.1029/2008JD010519.

Favier, V., M. Falvey, A. Rabatel, E. Praderio, and D. Lopez (2009). Interpreting discrepancies between discharge and precipitation in high-altitude area of Chile's Norte Chico region (26–32S).*Water Res.*, 45, W02424, doi:10.1029/2008WR006802.

Gardner, A. S., Sharp, M. J., Koerner, R. M., Labine, C., Boon, S., Marshall, S. J., Burgess, D. O., and Lewis, D. (2009), Near-surface temperature lapse rates over Arctic glaciers and their implications for temperature downscaling. *J. Clim.*, 22(16), 4281–4298, doi:10.1175/ 2009JCLI2845.1.

Grinsted, A. (2013). An estimate of global glacier volume. *The Cryosphere* 7, 141–151.

Harlow, R. C., Burke, E. J., Scott, R. L., Shuttleworth, W. J., Brown, C. M., and Petti, J. R. (2004). Derivation of temperature lapse rates in semi-arid southeastern Arizona. *Hydrol. Earth Syst. Sci.*, 8, 1179–1185.

Leclercq, P. W. and J. Oerlemans (2012). Global and hemispheric temperature reconstruction from glacier length fluctuations. *Clim. Dyn.* 38 1065-1079, doi: 10.1007/s00382-011-1145-7

Liston, G. E. and Elder, K. (2006). A meteorological distribution system for high-resolution terrestrial modeling (MicroMet). *J. Hydrometeorol.*, 7: 217–234.

Lundquist, J. D., and Cayan, D. R. (2007). Surface temperature patterns in complex terrain: Daily variations and long-term change in the central Sierra Nevada, California. *J. Geophys. Res.*, 112, D11124.

Malmros, J. K., Mernild, S. H., Wilson, R., Fensholt, R., & Yde, J. C. 2016. Glacier changes in the Rio Olivares catchment, central Chilean Andes, 1955–2013. *Journal of Glaciology*, 62(232) 391–401, doi: 10.1017/jog.2016.43.

Masiokas, M. H., Rivera, A., Espizua, L. E., Villalba, R., Delgado, S., and Aravena, J. C. (2009). Glacier fluctuations in extratropical South America during the past 1000 years, *Palaeogeogr. Palaeocl.* 281, 242–268.

Mernild, S. H., Liston, G. E., and Hiemstra, C. A. (2014). Northern Hemisphere glaciers and ice caps surface mass balance and contribution to sea-level rise. *J. Clim.* 27, 6051–6073, doi.org/10.1175/JCLI-D-13-00669.1.

Mernild, S. H., Liston, G. E., Hiemstra, C. A., Malmros, J. K., Yde, J. C., and McPhee, J. (2016). The Andes Cordillera. Part I: Snow Distribution, Properties, and Trends (1979–2014). *International Journal of Climatology*, doi:10.1002/joc.4804.

Mernild, S. H., Beckerman, A. P., Yde, J. C., Hanna, E., Malmros, J. K., Wilson, R., and Zemp, M. (2015). Mass loss and imbalance of glaciers along the Andes to the sub-Antarctic islands. *Glob. Planet. Change* 103, 109-119, doi.org/10.1016/j.gloplacha.2015.08.009.

Minder, J. R., Mote, P. W., and Lundquist, J. D. 2010. Surface temperature lapse rates over complex terrain: lessons from the Cascade Mountains. *J. Geophys Res*, 115:D14122, doi:10.1029/2009JD013493.

Oerlemans, J., Dyurgerov, M., and van de Wal, R. S. W. (2007). Reconstructing the glacier contribution to sea-level rise back to 1850. *The Cryosphere* 1, 59–65, doi:10.5194/tc-1-59-2007.

Pagès, M. and Miró, J.R. 2010. Determining temperature lapse rates over mountain slopes using vertically weighted regression: a case study from the Pyrenees. *Meteorol. Appl.*, 17, 53-63, doi, 10.1002/met.160.

Pepin, N., Benham, D., and Taylor, K. 1999. Modeling lapse rates in the maritime uplands of northern England: Implications for climate change. *Arct. Antarct. Alp. Res.*, 31, 151–164.

Rabatel, A., Castebrunet, H., Favier, V., Nicholson, L., and Kinnard, C. (2011). Glacier changes in the Pascua-Lama region, Chilean Andes (29°S): recent mass balance and 50 yr surface area variations. *The Cryosphere* 5, 1029–1041, doi:10.5194/tc-5-1029-2011.

Rabatel, A., et al. (2013). Current state of glaciers in the tropical Andes: a multi-century perspective on glacier evolution and climate change. *The Cryosphere* 7, 81–102, doi:10.5194/tc-7-81-2013.

Shea, J. M., Marshall, S. J., and Livingston, J. L. (2004). Glacier distributions and climate in the Canadian Rockies. *Arct. Antarct. Alp. Res.*, 36(2), 272–280.

World Glacier Monitoring Service (WGMS) (2012) *Fluctuations of Glaciers 2005–930 2010 (Vol. X)*, edited by: Zemp, M., Frey, H., Gärtner-Roer, I., Nussbaumer, S. U., 931 Hoelzle, M., Paul, F., and Haeberli W., ICSU (WDS) / IUGG (IACS) / UNEP / 932 UNESCO / WMO, World Glacier Monitoring Service, Zurich, Switzerland, 336 pp., 933 Publication based on database version: doi:10.5904/wgms-fog-2012-11.

Yang, Z., Hanna, E., Callaghan, T. V., and Jonasson, C. (2012). How can meteorological observations and microclimate simulations improve understanding of 1913–2010 climate change around Abisko, Swedish Lapland? *Met. Apps.* 19, 454–463. doi: 10.1002/met.276.

Table 1: TinyTag air temperature stations on Olivares Gamma Glacier. The surface elevation, slope, and aspect are obtained from the SRTM (Shuttle Radar Topography Mission), February 2000.

Station ID	Grid, UTM Zone 19 H	Grid	Elevation (m a.s.l.)	Slope SRTM (degree)	Aspect SRTM (degree)	Sensor ID, 1-m above surface	Sensor ID, 2-m above surface	Observed time period, begin (UTM time)	Observed time period, end (UTM time)	Sampling interval
Station 1	389375	6335136	4,492	7.8	127 (SE)	S9	S4	19/3; 4:00 pm	27/3; 10:00 am	Every minute
Station 2	391092	6334010	4,193	7.2	171 (S)	S8	S3	19/3; 4:40 pm	27/3; 10:00 am	Every minute
Station 3	391056	6333803	4,118	10.4	168 (S)	S10	S5	19/3; 5:30 pm	27/3; 10:00 am	Every minute
Station 4	391397	6332541	3,852	9.0	163 (S)	S7	S6	20/3; 12:15 pm	27/3; 10:00 am	Every minute
Station 5	391848	6331598	3,675	7.4	163 (S)	S1	S2	21/3; 4:50 pm	27/3; 10:00 am	Every minute

Table 2: Comparison of surface air temperature (°C) mean hourly data for 22–26 March 2015 at DGA and the five Tinytag sites (2-m sensors). See Figure 1 and Table 1 for site details. Hours with nocturnal observations are highlighted in italic (https://www.timeanddate.com/sun/chile/santiago), here illustrated in UTC.

Hour (UTC)	DGA	S2	S6	S5	S3	S4
0	3.8	2.1	0.1	-1.6	-1.5	-4.0
1	3.1	2.0	0.3	-1.8	-1.8	-4.2
2	2.7	1.3	-0.2	-2.1	-1.9	-4.3
3	2.2	1.5	-0.5	-2.1	-1.9	-4.4
4	1.7	2.2	0.2	-2.0	-2.1	-4.6
5	2.1	1.6	0.0	-2.4	-2.4	-4.8
6	2.1	1.1	-0.4	-2.7	-2.6	-5.1
7	1.8	0.5	-1.1	-3.3	-3.3	-5.4
8	1.3	0.1	-1.5	-3.5	-3.3	-5.5
9	0.6	0.0	-1.7	-3.4	-3.2	-5.9
10	0.2	0.2	-1.5	-3.6	-3.4	-5.9
11	*0.5*	*-0.1*	*-1.7*	*-3.6*	*-3.4*	*-5.9*
12	0.6	0.3	-1.1	-3.1	-2.9	-4.8
13	0.5	1.8	0.5	-1.9	-1.5	-2.9
14	0.9	3.6	2.3	0.1	-0.2	-2.2
15	2.3	6.9	4.6	1.8	1.7	-1.3
16	4.1	7.6	6.1	3.1	4.0	0.2
17	5.4	8.5	8.1	3.7	4.2	1.0
18	7.0	5.7	6.0	3.5	5.6	0.7
19	6.8	4.8	4.3	2.6	3.9	-0.9
20	4.8	3.6	2.3	-0.2	-0.1	-2.4
21	4.4	3.1	1.7	-1.0	-0.7	-3.0
22	3.3	1.6	0.5	-1.9	-1.8	-4.3
23	2.8	0.9	-0.8	-2.9	-2.8	-5.4
MEAN	2.7	2.5	1.1	-1.2	-0.9	-3.6
ST DEV	1.9	2.5	2.8	2.4	2.7	2.1

Table 3: Comparison of mean hourly lapse rate data (°C km^{-1}) for 22–26 March 2015 at the five Tinytag sites (2-m sensors). See Figure 1 and Table 1 for site details. Hours with nocturnal observations are highlighted in italic (https://www.timeanddate.com/sun/chile/santiago), here illustrated in UTC.

Hour (UTC)	LR(S4 -S2)	LR(S3 -S2)	LR(S5 -S2)	LR(S6 -S2)	LR(S4 -S6)	LR(S3 -S6)	LR(S5 -S6)	LR(S4 -S5)	LR(S4 -S3)
0	-7.4	-6.8	-8.3	-10.9	-6.4	-4.7	-6.5	-6.3	-8.3
1	-7.6	-7.4	-8.5	-9.8	-7.0	-6.1	-7.6	-6.6	-8.0
2	-6.9	-6.2	-7.6	-8.7	-6.4	-4.9	-6.9	-6.0	-8.0
3	-7.2	-6.5	-8.1	-10.9	-6.2	-4.3	-6.3	-6.1	-8.4
4	-8.3	-8.3	-9.6	-11.4	-7.5	-6.7	-8.4	-6.9	-8.3
5	-7.9	-7.9	-9.1	-9.1	-7.5	-7.2	-9.0	-6.4	-7.8
6	-7.7	-7.3	-8.7	-8.7	-7.4	-6.5	-8.7	-6.5	-8.3
7	-7.2	-7.3	-8.6	-9.2	-6.6	-6.3	-8.2	-5.4	-7.0
8	-6.9	-6.6	-8.2	-9.2	-6.2	-5.3	-7.5	-5.3	-7.4
9	-7.2	-6.1	-7.6	-9.5	-6.6	-4.4	-6.3	-6.8	-9.2
10	-7.4	-6.9	-8.4	-9.6	-6.8	-5.5	-7.6	-6.3	-8.3
11	-7.2	-6.5	-8.0	-9.3	-6.6	-5.1	-7.1	-6.2	-8.3
12	-6.2	-6.2	-7.6	-7.8	-5.7	-5.3	-7.4	-4.5	-6.1
13	-5.8	-6.5	-8.3	-7.7	-5.3	-5.9	-8.8	-2.7	-4.5
14	-7.0	-7.3	-7.9	-7.4	-6.9	-7.2	-8.3	-5.9	-6.6
15	-10.0	-10.1	-11.5	-13.0	-9.2	-8.6	-10.5	-8.3	-9.8
16	-9.0	-7.0	-10.0	-8.6	-9.1	-6.1	-11.0	-7.8	-12.5
17	-9.1	-8.3	-10.8	-2.1	-11.0	-11.5	-16.6	-7.1	-10.5
18	-6.2	-0.3	-5.0	1.5	-8.3	-1.2	-9.3	-7.5	-16.3
19	-7.0	-1.9	-5.1	-3.2	-8.1	-1.1	-6.4	-9.3	-16.0
20	-7.4	-7.1	-8.6	-7.1	-7.4	-7.1	-9.6	-5.9	-7.8
21	-7.5	-7.3	-9.2	-8.0	-7.4	-6.9	-10.0	-5.5	-7.9
22	-7.2	-6.7	-8.1	-6.6	-7.4	-6.7	-9.1	-6.3	-8.2
23	-7.7	-7.1	-8.5	-9.6	-7.2	-5.8	-7.8	-6.8	-8.8
MEAN	-7.5	-6.6	-8.4	-8.2	-7.3	-5.9	-8.5	-6.4	-8.9
STDEV	0.9	1.9	1.4	3.1	1.2	2.1	2.2	1.3	2.7

Table 4: Correlation coefficients between surface air temperatures recorded by the Tinytags and meteorological parameters recorded at the DGA automatic weather station, based on hourly data from 21:00 on 21 March to 13:00 on 27 March 2015. Correlations ≥0.5 or ≤-0.5 are highlighted in bold.

	Air temp.	Rel. humidity	Wind direction	Wind speed	Snow depth	Air pressure	Incoming shortwave	Incoming longwave	Outgoing longwave	Reflected shortwave
2-m Tinytags										
S2	**0.78**	-0.43	0.02	0.30	0.08	**0.53**	**0.61**	0.16	**0.71**	0.39
S6	**0.75**	-0.34	-0.09	0.25	0.09	0.41	**0.67**	0.24	**0.70**	0.38
S5	**0.71**	-0.24	-0.17	0.19	0.08	0.34	**0.62**	0.35	**0.69**	0.28
S3	**0.66**	-0.22	-0.17	0.18	0.08	0.29	**0.63**	0.30	**0.66**	0.28
S4	**0.71**	-0.25	-0.18	0.21	0.05	0.35	**0.59**	0.36	**0.70**	0.24
1-m Tinytags										
S1	**0.76**	-0.39	-0.01	0.28	0.05	0.51	**0.60**	0.19	**0.68**	0.43
S7	**0.72**	-0.28	-0.13	0.21	0.06	0.38	**0.64**	0.29	**0.67**	0.39
S10	**0.66**	-0.18	-0.21	0.14	0.06	0.29	**0.61**	0.37	**0.65**	0.31
S8	**0.70**	-0.24	-0.18	0.20	0.07	0.32	**0.66**	0.33	**0.69**	0.32
S9	**0.69**	-0.21	-0.21	0.18	0.05	0.32	**0.55**	0.41	**0.68**	0.20

Table 5: Comparison of mean hourly 2-m minus 1-m temperature differences (°C) for 22–26 March 2015 at the five Tinytag sites. Differences ≥0.5 °C are highlighted in bold. See Figure 1 and Table 1 for site details. Hours with nocturnal observations are highlighted in italic (https://www.timeanddate.com/sun/chile/santiago), here illustrated in UTC.

Hour (UTC)	S2-S1	S6-S7	S5-S10	S3-S8	S4-S9
0	0.3	0.2	0.2	0.2	0.2
1	0.3	0.3	0.2	0.2	0.2
2	0.3	0.3	0.2	0.2	0.1
3	0.4	0.3	0.1	0.2	0.2
4	0.4	0.2	0.2	0.1	0.2
5	0.4	0.3	0.2	0.3	0.2
6	0.4	0.4	0.2	0.2	0.3
7	0.3	0.2	0.2	0.2	0.3
8	0.2	0.2	0.2	0.3	0.2
9	0.3	0.2	0.2	0.1	0.2
10	0.3	0.3	0.3	0.2	0.2
11	0.3	0.2	0.3	0.2	0.2
12	0.3	0.3	0.2	0.1	0.3
13	0.3	**0.7**	0.3	-0.1	0.1
14	0.4	**0.6**	0.1	-0.5	0.3
15	0.4	0.3	-0.4	-0.4	0.4
16	0.1	-0.1	-0.7	0.3	**0.7**
17	0.1	**0.6**	-0.7	0.1	**0.9**
18	**0.5**	**1.3**	-0.7	**1.1**	**1.1**
19	**0.5**	0.3	-0.1	**1.0**	**0.7**
20	0.4	**0.6**	0.1	-0.2	**0.5**
21	0.4	0.4	0.1	0.1	0.1
22	0.2	**0.5**	0.1	0.0	0.1
23	0.2	0.2	0.2	0.1	0.3
MEAN	0.3	0.4	0.0	0.2	0.3
ST DEV	0.1	0.3	0.3	0.3	0.3

Table 6: Daily and mean daily (22–26 March 2015) temperatures (°C) for all ten Tinytag sensors (1-m and 2-m elevation at five sites) based on 1-min data.

	22 Mar	23 Mar	24 Mar	25 Mar	26 Mar	Mean daily
2-m Tinytags						
S2	4.6	4.2	2.1	1.3	0.2	2.5
S6	2.7	2.4	1.6	0.3	-1.6	1.1
S5	0.0	-0.3	-0.4	-1.6	-3.9	-1.2
S3	0.0	-0.1	0.1	-1.1	-3.9	-1.0
S4	-2.3	-2.5	-3.3	-3.8	-6.1	-3.6
1-m Tinytags						
S1	4.1	3.8	2.0	0.9	0.1	2.2
S7	2.0	1.8	1.4	-0.1	-1.8	0.6
S10	-0.3	-0.6	-0.1	-1.5	-4.0	-1.3
S8	0.0	-0.1	-0.3	-1.5	-3.7	-1.2
S9	-2.9	-2.8	-3.4	-4.2	-6.4	-3.9

Table 7: Daily and mean daily lapse rates (°C km^{-1}) between various pairs of Tinytag sensors based on 1-min data.

	22 Mar	23 Mar	24 Mar	25 Mar	26 Mar	Mean daily
2-m Tinytags						
S4-S2	-8.5	-8.5	-6.6	-6.3	-7.7	-7.4
S3-S2	-8.8	-8.8	-3.9	-4.8	-8.0	-6.7
S5-S2	-10.5	-10.5	-5.7	-6.5	-9.2	-8.4
S6-S2	-10.9	-10.9	-3.1	-5.9	-10.3	-8.1
S4-S6	-7.8	-7.8	-7.6	-6.4	-7.0	-7.3
S3-S6	-7.7	-7.7	-4.4	-4.2	-6.9	-6.0
S5-S6	-10.2	-10.2	-7.4	-7.0	-8.5	-8.6
S4-S5	-6.2	-6.2	-7.7	-6.0	-5.9	-6.3
S4-S3	-8.0	-8.0	-11.2	-9.0	-7.1	-8.7
1-m Tinytags						
S9-S1	-8.5	-8.5	-6.6	-6.2	-7.9	-7.5
S8-S1	-8.0	-8.0	-4.5	-4.7	-7.4	-6.4
S10-S1	-9.9	-9.9	-4.7	-5.3	-9.3	-7.8
S7-S1	-11.9	-11.9	-3.3	-5.9	-10.6	-8.6
S9-S7	-7.6	-7.6	-7.6	-6.3	-7.2	-7.1
S8-S7	-5.9	-5.9	-5.0	-4.1	-5.7	-5.2
S10-S7	-8.5	-8.5	-5.7	-4.9	-8.3	-7.2
S9-S10	-6.9	-6.9	-8.9	-7.2	-6.3	-7.1
S9-S8	-9.4	-9.4	-10.4	-8.8	-8.8	-9.3

Table 8: A comparison of mean temperatures and the spread of temperature values (standard deviation = ST DEV) (°C) recorded by LogTag and Tinytag instruments, based on 2-min data for 22–26 March, 2015.

	LogTag mean (ºC)	Tinytag mean (ºC)	Mean temperature difference (Logtag-Tinytag)	LogTag ST DEV	Tinytag ST DEV
2-m Tinytags					
S2	2.7	2.5	0.2	2.5	2.4
S6	1.2	1.0	0.1	2.6	2.7
S5	-1.1	-1.2	0.1	2.4	2.3
S3	-1.2	-1.0	-0.2	2.2	2.6
S4	-3.5	-3.6	0.1	2.3	2.1
1-m Tinytags					
S1	2.3	2.2	0.2	2.3	2.4
S7	1.2	0.6	0.5	2.9	2.5
S10	-1.3	-1.3	0.0	2.3	2.6
S8	-0.9	-1.1	0.3	2.5	2.6
S9	-3.6	-3.9	0.3	2.2	2.0

Figure 1: Location of Olivares Gamma Glacier, and of meteorological stations used in the study. Topographic details of stations are given in Table 1; numbers 1–10 after the colons refer to Tinytag sensor IDs.

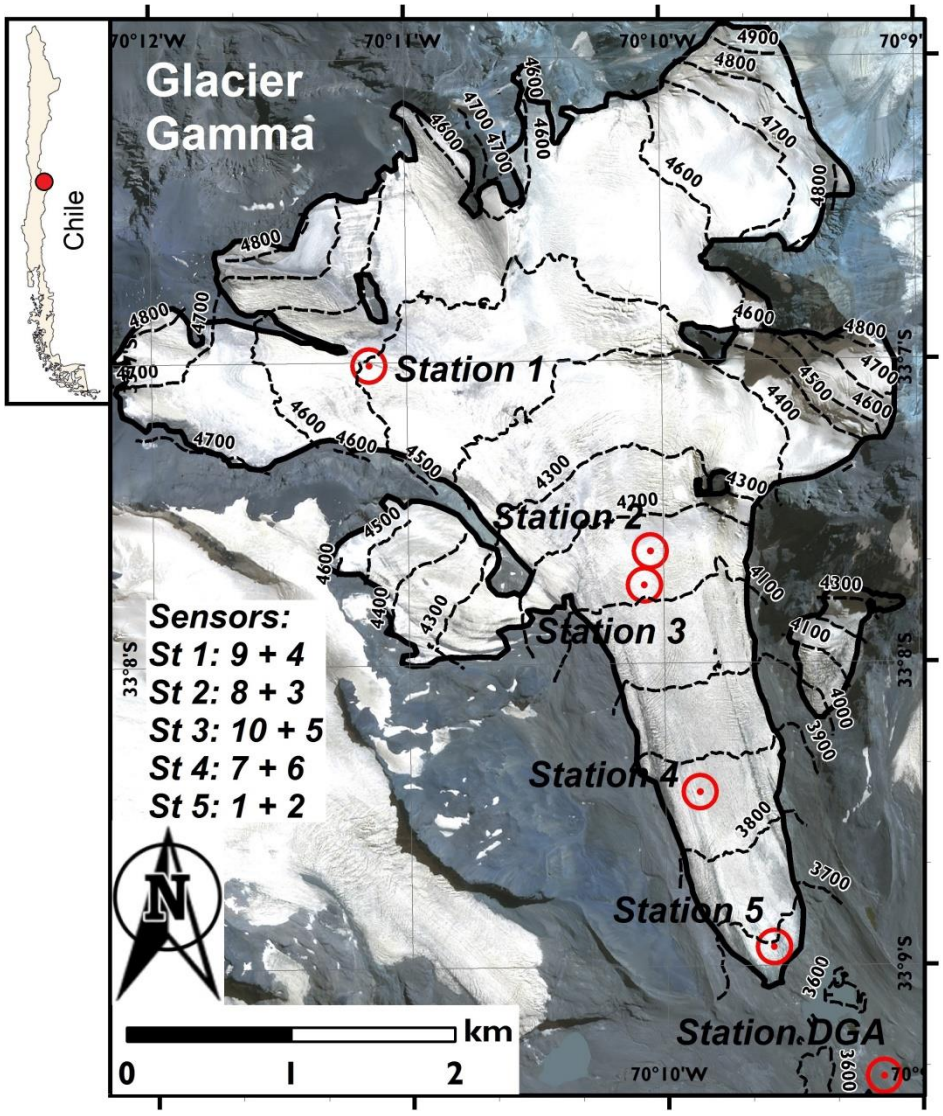

Figure 2: (a) Photos of Olivares Gamma Glacier taken from drone looking north [the distance between Stations 3 and 4 is approximately one kilometre]; (b) Station 3 at 4118-m elevation with Tinytag sensors 10 and 5 at 1 m and 2 m heights; (c) Station 4 at 3,852-m elevation with Tinytag sensors 7 and 6 at 1 m and 2 m heights. Photo (a) was stitched together, (b) was taken by J. C. Yde and (c) by E. Hanna.

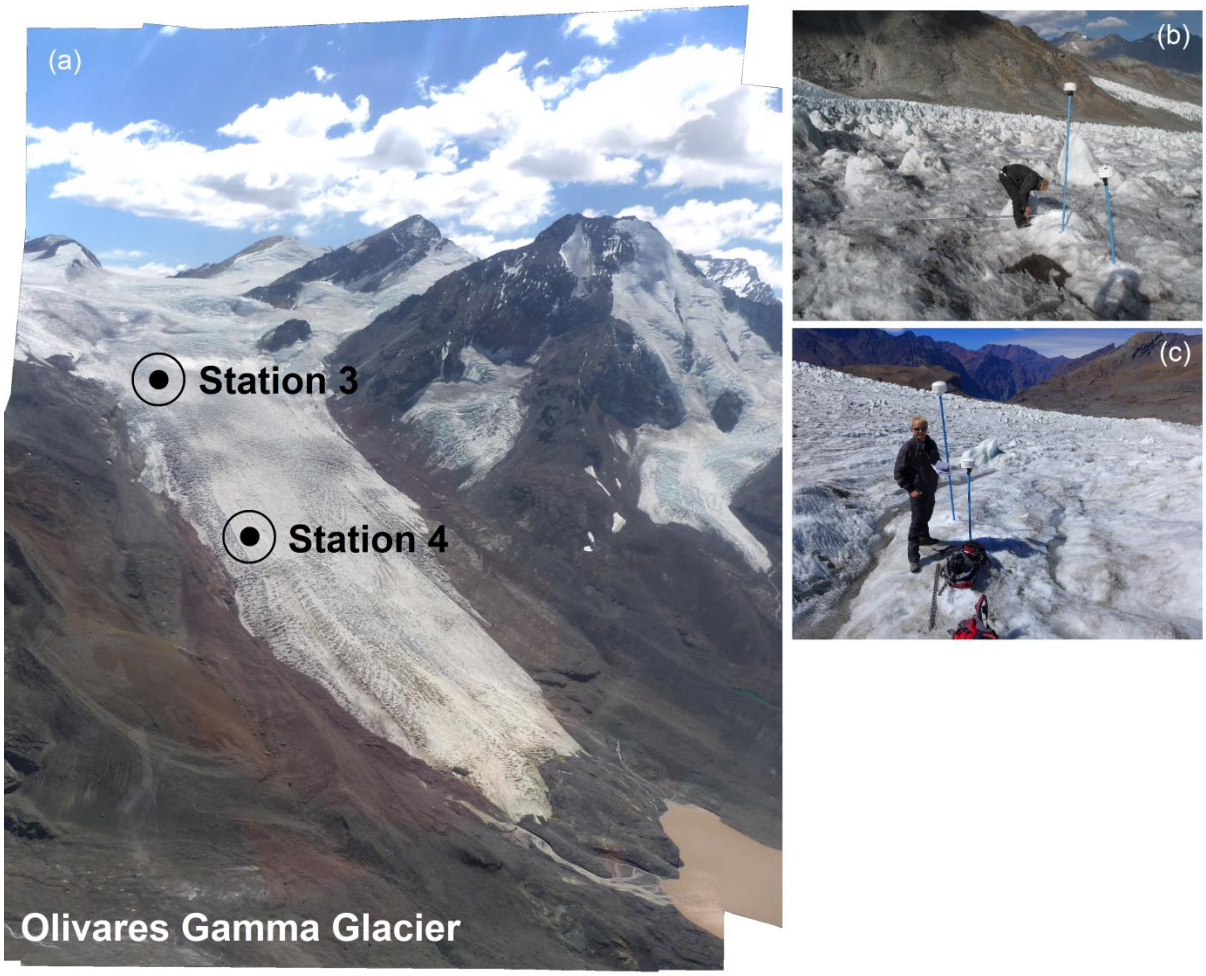

Figure 3: DGA automatic weather station time series from March 19–26 2015: (a) surface air temperature and relative humidity; (b) mean sea-level pressure; (c) wind speed and wind direction; and (d) incoming (black) and reflected (blue) shortwave radiation, and incoming (red) and outgoing (green) longwave radiation.

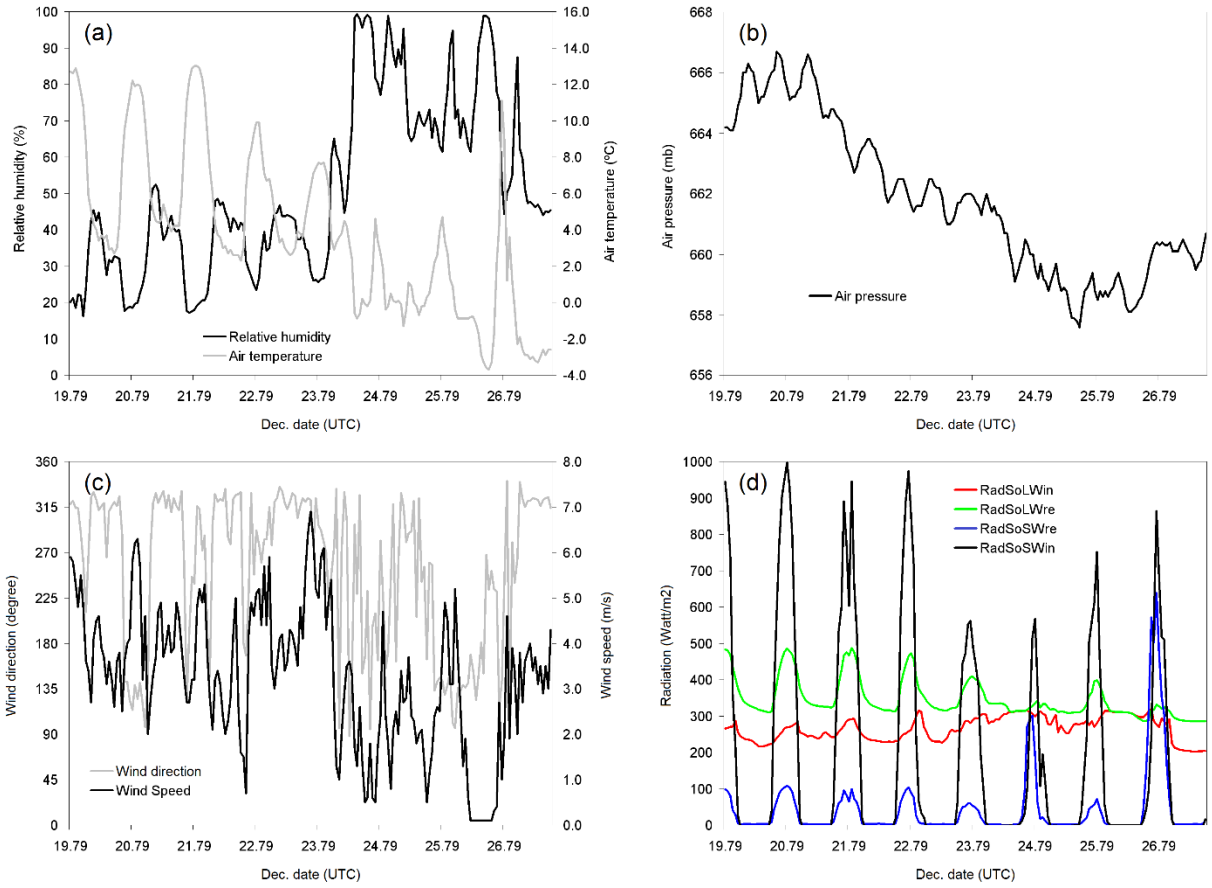

Figure 4: (a) 2-m surface air temperature profiles at the DGA automatic weather station and Tinytag sensors S2, S6, S5, S3 and S4 (moving progressively up the glacier), based on data recorded each hour (19–26 March 2015); and (b) mean daily 2-m surface air temperature profiles (22–26 March 2015) for the same stations/sensors as in Figure 4a.

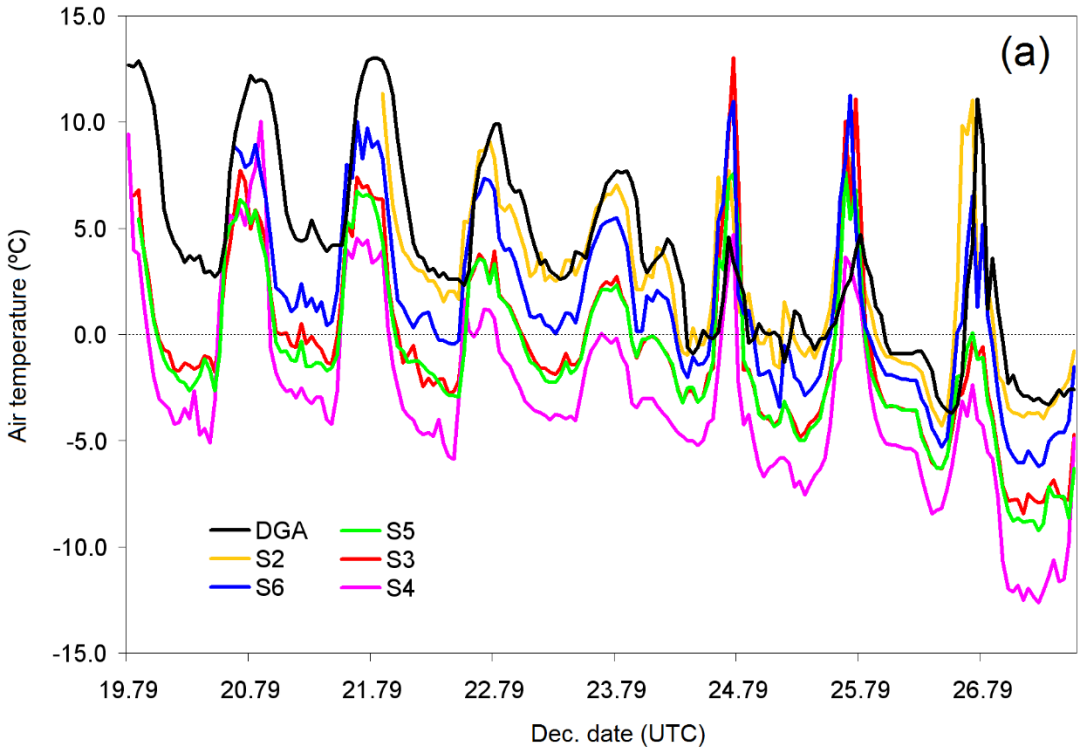

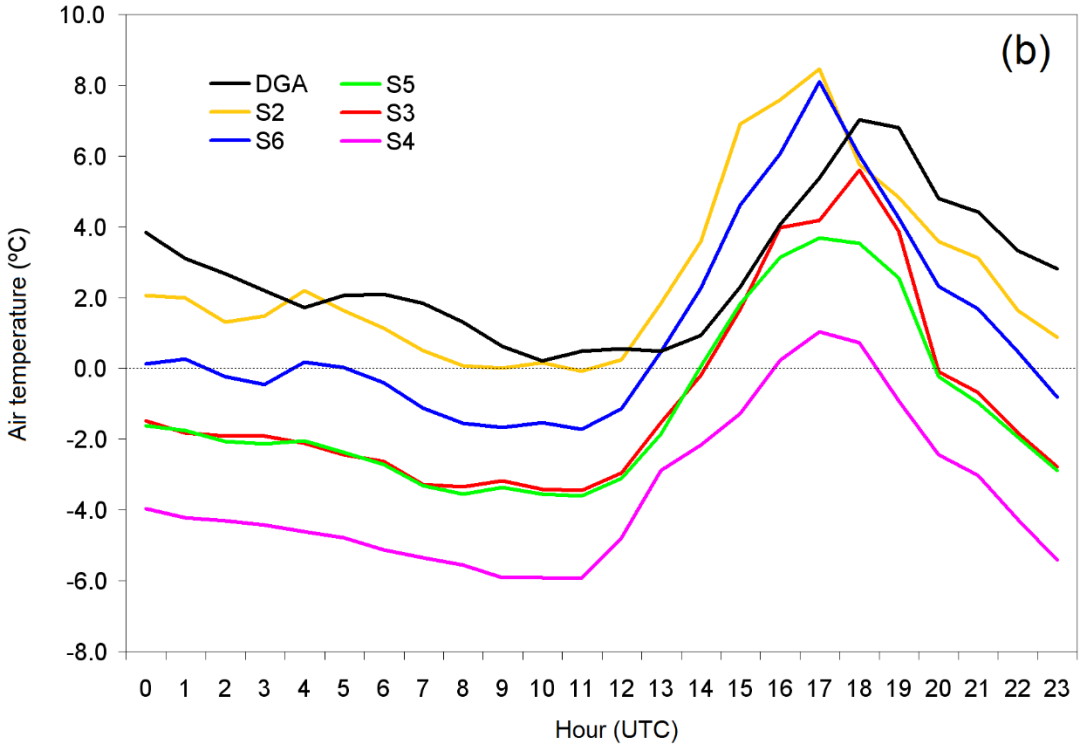

Figure 5: (a) Temperature differences between 2 m and 1 m above the glacier surface (19–26 March 2015), as recorded by the Tinytags at the five glacier stations (Figure 1); and (b) mean daily profiles (22–26 March 2015) of the data shown in Figure 5a.

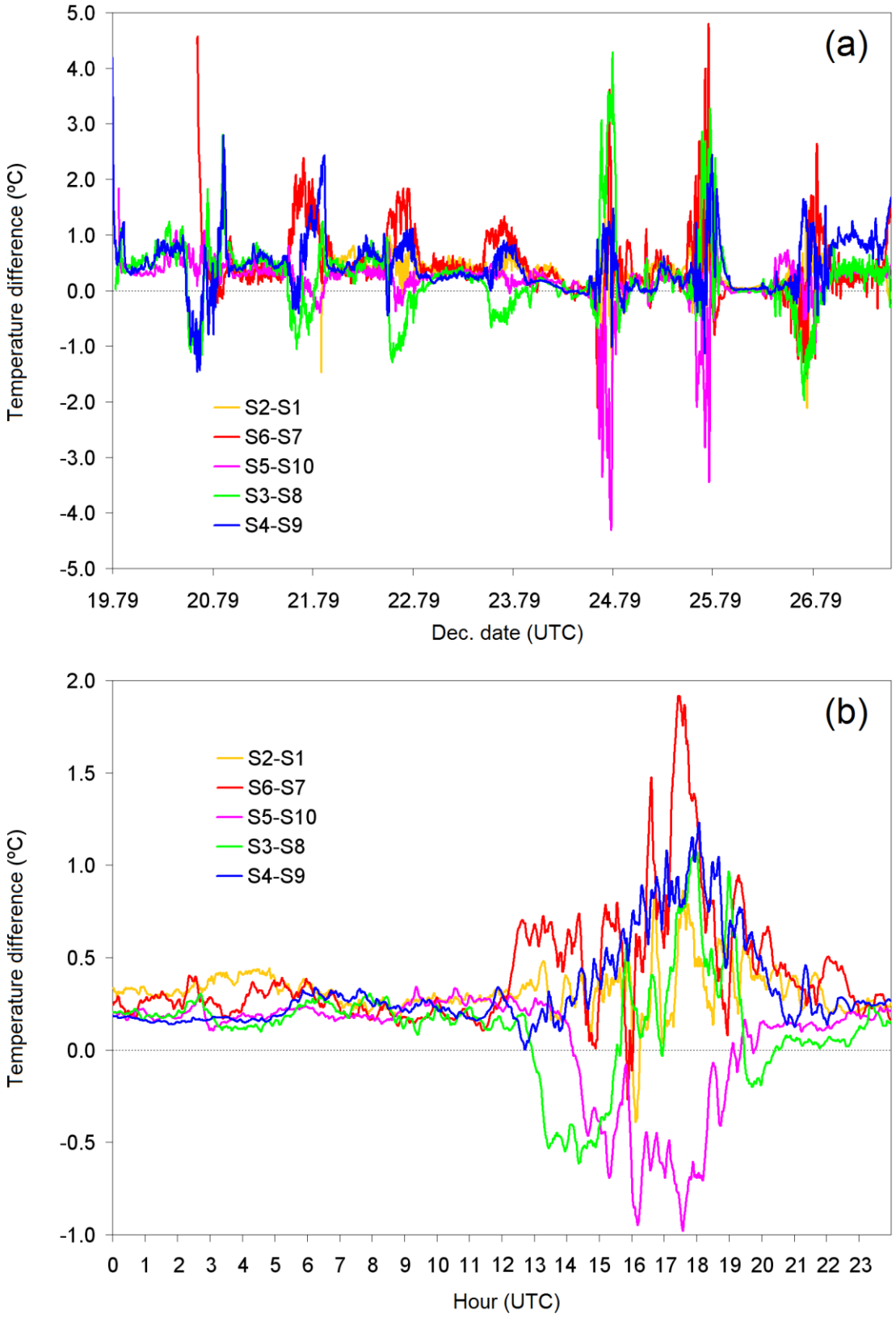

Figure 6: (a) 2-m surface air temperature profiles at the Tinytag sensors S2, S6, S5, S3 and S4 (moving progressively up the glacier), based on 1-min data; (b) 1-m surface air temperature profiles at the Tinytag sensors S1, S7, S10, S8 and S9 (moving progressively up the glacier), based on 1-min data; (c) mean daily 2-m surface air temperature profiles (22–26 March 2015) for the same stations/sensors as in Figure 6a; and (d) mean daily 1-m surface air temperature profiles (22–26 March 2015) for the same stations/sensors as in Figure 6b.

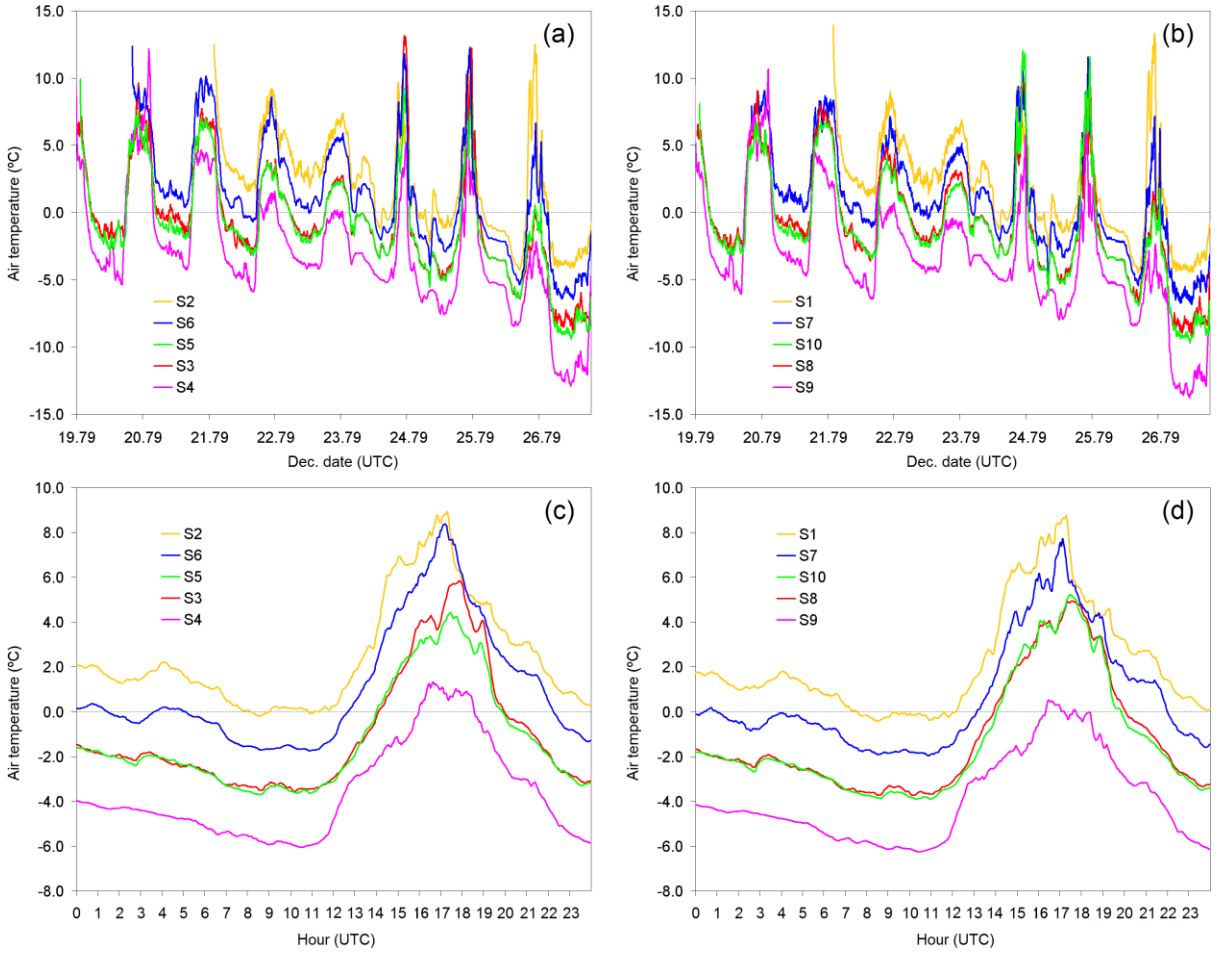

Figure 7: Near-surface glacier lapse-rate variations over time, at 2-m height above the glacier surface, based on 1-min Tinytag temperature data. Different base stations (Figure 1) are used as follows: (a) S2/Station 5 (near the bottom of the glacier); (b) S1/Station 5; (c) S6/Station 4; (d) S7/Station 4; and (e) lapse rates are for the upper half of the glacier (base Stations 2 and 3).

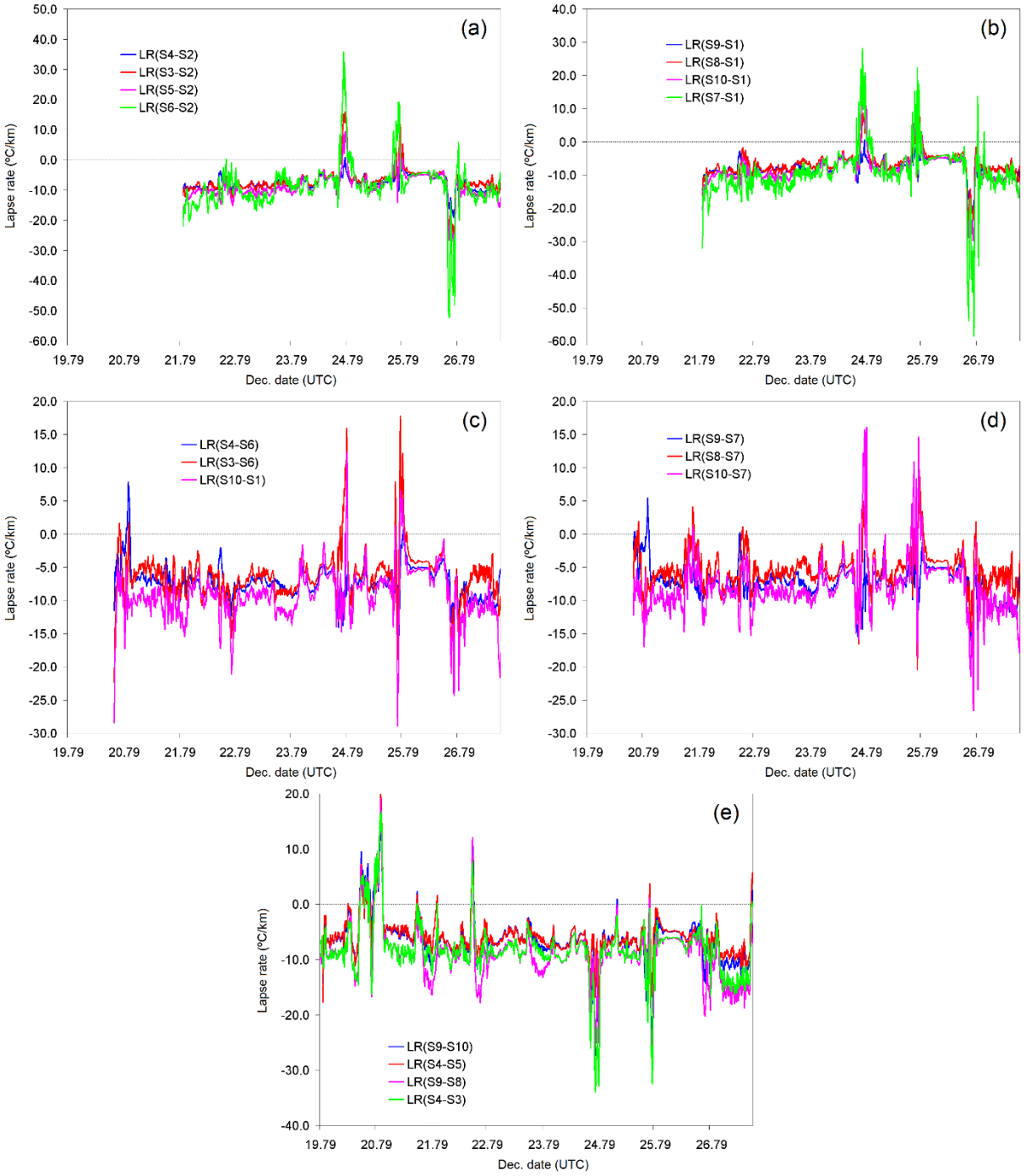

Figure 8: Mean daily profile (22–26 March 2015) of lapse-rate data in: (a) between Station S2 and other stations; (b) Station S1 and other stations; (c) Station S6 and other stations; (d) Station S7 and other stations; and (e) between different stations.